Experimental study of dispersed flow film boiling at sub-channel scale in LOCA conditions: Influence of the steam flow rate and residual power

A.V.S. Oliveira, J.D. Peña Carrillo, Alexandre Labergue, T. Glantz, Michel Gradeck

Experimental study of dispersed flow film boiling at sub-channel scale in LOCA conditions: influence of the steam flow rate and residual power

A. V. S. Oliveira[a,b], J. D. Peña Carrillo[a,b], A. Labergue[b], T. Glantz[a], M. Gradeck[b,*]

[a]*IRSN, PSN/SEMIA/LEMC, B.P. 3, 13115 Saint Paul-Lez-Durance, France*
[b]*LEMTA, UMR CNRS 7563, Université de Lorraine, Vandoeuvre-Lès-Nancy 54505, France*

Abstract

Reflooding experiments with rod bundles at Loss Of Coolant Accident (LOCA) conditions usually use intrusive methods with limited access and, consequently, their data are not always adequate and comprehensive to validate simulation codes. For this reason, sub-channel scale experiments are useful to obtain detailed data in a more controlled environment for an accurate thermal-hydraulics investigation. In this study, we present experiments of the cooling phase with an internal steam-droplets flow in a vertical pipe simulating an undamaged sub-channel in a nuclear reactor. Simultaneous measurements were performed of the wall temperature and droplets characteristics (velocity, diameter and temperature) using only optical techniques. An analysis is made on how the steam flow rate and maintained heating power during the cooling phase affect the wall heat dissipation, wall rewetting and droplets dynamics. Results show that wall rewetting normally occurs from bottom to top, and the temperature at minimum heat flux is highly affected by the droplets dynamics. Furthermore, droplets are accelerated when passing through the heated tube, especially at higher wall temperatures, and their temperature is nearly the same up- and downstream of the test section. Results with heating during the cooling phase show that wall rewetting takes place at higher wall temperatures and advances slower with the increase in the maintained heating power. Moreover, for the time period and flow conditions used in this work, wall rewetting does not occur for maintained powers higher than 1.5 kW/m.

Keywords:
Two-phase flow, LOCA, Thermal-hydraulics, Residual power, Infrared thermography, Droplets dynamics

Nomenclature

Greek letters

β	temperature sensitivity coefficient	$\dot{m}$	mass flow rate
ϕ	heat flux	a,b,c	3cLIF calibration parameters
ρ	density	Bi	Biot number
ρ_0	electrical resistivity	C_p	specific heat
σ	surface tension	D	diameter (tube)
		d	diameter (droplets)

Roman letters

h	heat transfer coefficient

---

*Corresponding author
Email address:* `michel.gradeck@univ-lorraine.fr` (M. Gradeck)

I	electrical current	x	arbitrary parameter
I_f	fluorescence intensity	z	axial position
k	thermal conductivity		

Subscripts

L	length	0	reference
M.H.P.	maintained heat power	1,2,3	spectral bands
N	amount of data	d	droplet
P	population	ext	external
R_f	fluorescence ratio	h	hydraulic diameter
S	cross-sectional area	int	internal
T	temperature		
t	time	loss	heat losses
u	velocity	s	steam
w	thickness	t	tube
We	Weber number	w	wall

1. Introduction

One of the design-related accidents of a Pressurized Water Reactor (PWR) is the Loss Of Coolant Accident (LOCA), whose initiating event is a breach in the primary circuit of the reactor leading to a loss of water inventory. Although emergency shutdown systems immediately interrupt the fission chain reaction, there is still a fuel residual power that may not be properly dissipated and, in the case of a large break where a large amount of water is lost, drying on the fuel assemblies can take place. Hence, the reactor's core temperature would still considerably increase, which may result in fuel rod claddings deformation and appearance of blocked zones. In a process known as reflooding phase, emergency core cooling systems (ECCS) inject water into the core to cool down the fuel assemblies, limiting its damage and preserving the reactor's structure during a LOCA. This injected subcooled liquid flows through the pipes of the primary circuit, then in the annular space of the vessel and finally reaches the bottom of the core. As the liquid injection continues, the water level rises and immerses the fuel assemblies, where we identify three zones with different flow conditions (Fig. 1): (i) the quenching front, corresponding predominantly to the nearly-saturated water below the water level and where the first boiling mechanisms are observed; (ii) a two-phase post-dryout zone composed of superheated steam and dispersed droplets; and, finally, (iii) a monophasic post-dryout zone of superheated steam when all the droplets disappear because of evaporation [1].

This demonstrates that the core's coolability analysis during the reflooding phase involves complex and highly coupled thermal-hydraulic phenomena, depending on both the steam and droplets characteristics, the water injection rate, the fuel cladding temperature, the fuel residual power to dissipate, and, if applicable, the damaged cladding geometry (blockage ratio, length and position) [2, 3]. For example, typical characteristics of the two-phase flow in LOCA conditions are [4–6]:
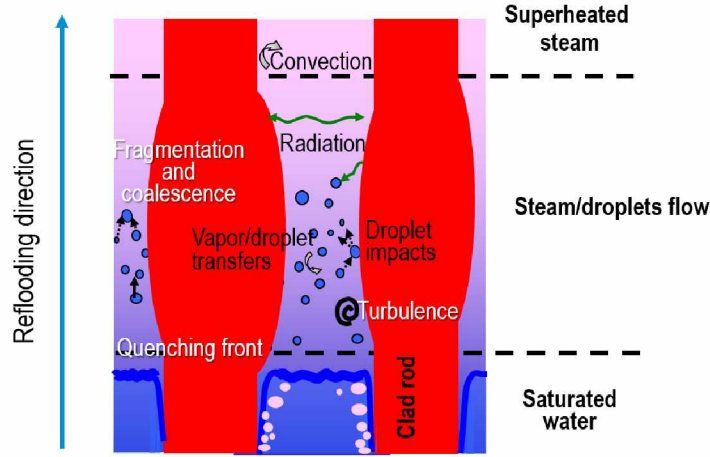
Figure 1: Transport phenomena during a LOCA [1].

- Droplets temperature: close to saturation;

- Droplets diameter: from 50 μm to 1000 μm;

- Volumetric fraction of liquid: from 10^{-4} to 10^{-2};

- Steam temperature: up to 800 °C;

- Steam pressure: up to 3 bar;

- Cladding temperature: from 300 °C to 1200 °C;

- Residual power per fuel rod: from 0.3 kW/m to 3 kW/m.

This region with steam-droplets flow is a typical dispersed flow film boiling situation, also called in the literature as post-CHF film boiling [7] or heat transfer with mist flow [8]. This phenomenon occurs when there is dry-out of the surface, i.e. no liquid film on the wall, and the vapor quality is less than one. Hence, liquid is still present in the flow but as dispersed droplets. This thermal-hydraulic process is found in many engineering applications like steam generators, spray cooling process and refrigeration systems [9]. The majority of dispersed flow film boiling studies are interested in estimating the surface temperature in this regime [7, 10], especially in refrigeration application where the heat transfer coefficient reduces after the liquid film over the surface vanishes. Other studies are interested in the heat dissipated by the flow and the quenching process, as found in spray cooling researches for metallurgy applications [11–13].

However, a great portion of the studies of dispersed flow film boiling concerns nuclear engineering, especially nuclear reactors. Although this is the same subject mentioned above, the difference between the wall and the flow temperatures is much higher in nuclear reactor applications compared with refrigeration, for example. If we compare nuclear and metallurgy applications of this phenomenon, the flow characteristics and involved geometries are completely different. For this reason, there is a dense literature of disperse flow film boiling specific for nuclear engineering applications [1, 5, 14–16], especially because this thermal-hydraulic process is very important to ensure the cooling of the fuel rods above the quenching front and, therefore, guarantee nuclear safety.

3

To deepen the understanding of the core cooling during a LOCA, the French Institute of Radiation Protection and Nuclear Safety (IRSN, in French) has launched, with the support of the French National Agency for Research, the project PERFROI [3], which is structured in two axes: thermal-mechanics (axis 1) and thermal-hydraulics (axis 2). The main experiment named COAL[1], which is planned in the latter axis, will provide measurements of the coolability with a partially ballooned 7x7 rods bundle during reflooding in LOCA conditions, especially observing the thermal-hydraulics in the ballooned region. Nevertheless, as in many similar experiments [2, 14, 15], this test has limited access to do the measurements and have to resort to intrusive instruments like thermocouples, which means only local information is collected. Moreover, this is more difficult to control the environment and have accurate, repetitive and detailed data in this sort of apparatus for the validation of mechanistic models.

To overpass these difficulties and to create a robust experimental database of dispersed flow film boiling, a new test rig named COLIBRI [2] was built to study the cooling process at sub-channel scale using only optical techniques on the test section (hence non-intrusive methods). With this apparatus, we are able to vary many conditions and blockage geometries and, as consequence, detailed parametric studies are performed to complement the results that COAL experiments will provide. Moreover, the obtained data are valuable for the validation of simulation tools, like IRSN's code called DRACCAR [17, 18], and understand with parameters play important roles on the thermal-hydraulics of dispersed flow film boiling. In a previous study, we correlated the flow characteristics with the wall temperature during the cooling phase and analyzed the blockage ratio effect on the heat dissipation and the droplets characteristics after testing tubes with different geometries [1].

The present work is a continuation of the experimental study of the cooling process at sub-channel scale with dispersed flow film boiling at LOCA conditions. The effect of two other important parameters are investigated: steam flow rate and maintained heating power (which simulates the fuel residual power during a LOCA). Here, a single tube represents an undamaged sub-channel for all the experiments and, therefore, the blockage ratio effect is not analyzed to avoid conjugated parametric effects. For each scenario, we evaluated the heat dissipation, wall rewetting position, and the droplets dynamics and temperature up- and downstream of the heated tube. Although this study is focused on nuclear engineering applications, this might also be interesting for refrigeration and metallurgy engineering, as well as applications of high-temperature heat exchangers like steam generators; especially results concerning heat dissipation and wall rewetting

2. Experimental set-up

2.1. Representation at sub-channel scale

The definition of a sub-channel in a PWR is the volume of fluid between four neighboring fuel rods, which can be represented by a single circular tube with the same hydraulic diameter D_h. Figure. 2 illustrates the case concerned in our study, which is a sub-channel created by undamaged rods with typical dimensions found in French PWRs, resulting in a hydraulic diameter of 11.78 mm. On the one hand, performing tests at sub-channel scale does not replicate the real geometry. In fact, the sub-channel representation is a closed system, so it does not consider

---

[1]COAL: **CO**olability of a fuel **A**ssembly during **L**OCA
[2]COLIBRI: **CO**o**LI**ng of **B**lockage **R**egion **I**nside a PWR Reactor

any sort of exchange and interaction between neighboring sub-channels. Moreover, because of the different channel geometry, the steam flow might behave differently compared to the real condition, which might affect the droplets behavior as well. On the other hand, since the present study concerns an undamaged geometry (that means no blockage), considering the sub-channel as an isolated system is reasonable because the flow occurs preferably in the axial direction. Also, this method allows great control of the environmental and test conditions, as well as detailed parametric analysis of the thermal-hydraulics throughout the cooling process.
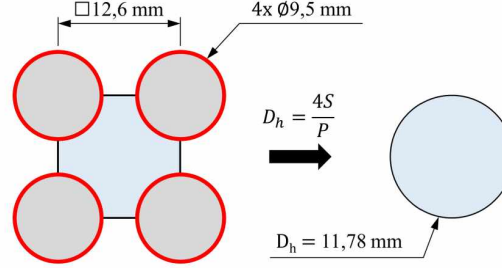

Figure 2: Sub-channel representation of a PWR.

2.2. Configuration of the experimental apparatus

Figure 3 presents the experimental set-up, which consists of a test section, a droplet supply system and a super-heated steam supply system. This apparatus is the same used in previous works [1, 19].
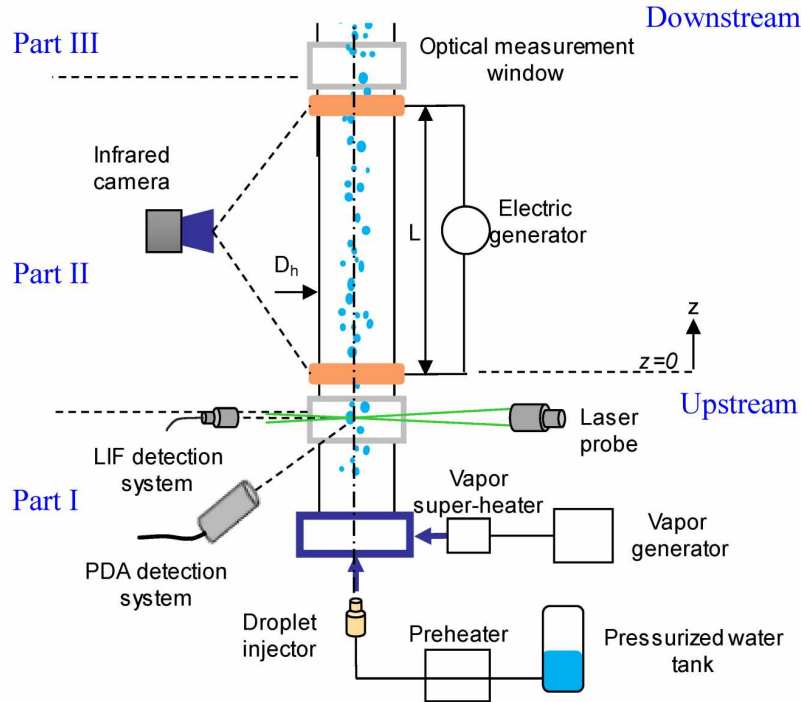

Figure 3: Schematic diagram of COLIBRI experimental set-up.

The test section is made of Inconel-625 and is divided into three parts: Parts I and III are fixed tubes with 0.57 mm wall thickness and an internal diameter D_h of 11.78 mm, reproducing, respectively, a typical rod cladding thickness and to the nominal hydraulic diameter of an undamaged PWR sub-channel, as shown in Fig. 2. Part II is exchangeable, which allows to investigate the blockage ratio effect as presented in previous works [1, 19]. However, in this study we use only a straight tube as Part II that has a length L of 170 mm and, like the other parts, has 0.57 mm wall thickness and 11.78 mm internal diameter. Moreover, Part II is heated by Joule effect with the use of a DC power supply (TDK LAMBDA 2U-3300®).

A steam generator and a super-heater (AURA®) in one line provide water vapor at temperatures up to 200 °C and with a maximum flow rate of 10 kg/h. In another line, a piezoelectric injector (FMP Technology®) produces droplets with diameters up to 500 μm at a constant flow rate of 0.8 kg/h. These two lines meet in a mixer whose outlet supplies the dispersed steam-droplets two-phase flow upstream of Part I. The length of the tube used in this part is approximately 300 mm long, ensuring a developed flow in the zone of interest (Part II).

2.3. Optical techniques

Optical accesses up- and downstream of Part II allow the measurement of the droplets characteristics: diameter, axial velocity and temperature. Their diameter and axial velocity are measured by a Phase-Doppler Analyzer (PDA) manufactured by Dantec Dymanics® [20]. This system includes a classic PDA reception optics and a P80 signal processor. An LDA transmitter probe (Dantec-Dynamics Fiber Flow®) generates the laser excitation volume with the green line (514.5 nm wavelength) of an argon-ion laser. Moreover, this system operates in the first-refraction mode with a 60° off-axis angle, with the focal lengths of the transmitter and the receiver being 1200 mm and 310 mm, respectively. This optical configuration allows us to measure droplets diameters up to 300 μm. We used a spherical validation of 25%, which rejects not more than 10% of the detected droplets. The uncertainty of a PDA-system is not evident to calculate, so this is estimated by statistical analysis [21, 22], which gives 10% uncertainty in the droplets diameter and 5% in the droplets axial velocity.

Meanwhile, the droplets mean volume temperature is measured by Laser-Induced Fluorescence (LIF) thermometry, which works because of a dye dissolved in water whose fluorescence intensity is temperature-dependent. This technique and its details have been exhaustively presented in previous works [1, 23, 24]. Usually, LIF thermometry estimates the fluid temperature by using a first ratio R_f of fluorescence intensities I_f collected simultaneously in two different spectral bands 1 and 2 having different temperature sensitivities (so $R_{f12} = I_{f1}/I_{f2}$). Thus, the temperature measurement is free of several parametric effects like dye concentration, collection volume, laser excitation intensity and optical layout. However, in the presence of a polydisperse population of droplets, it is necessary to eliminate as well the droplet size effect [23, 24], so a third spectral band is used for this purpose. This technique is referred as 3cLIF (three-color LIF) thermometry. By obtaining a second ratio of fluorescence $R_{f32} = I_{f3}/I_{f2}$, which is mainly sensitive to the droplet diameter, we find the following implicit equation for the droplets mean volume temperature T_d that is only dependent on both measured fluorescence ratios [23]:

$$\frac{R_{f12}}{R_{f120}} e^{\beta_{12}\left(\frac{1}{T_0} - \frac{1}{T_d}\right)} = a \left[e^{\beta_{32}\left(\frac{1}{T_0} - \frac{1}{T_d}\right)} \frac{R_{f32}}{R_{f320}} \right]^2 + b \left[e^{\beta_{32}\left(\frac{1}{T_0} - \frac{1}{T_d}\right)} \frac{R_{f32}}{R_{f320}} \right] + c \qquad (1)$$

where β_{12} and β_{32} are temperature sensitivity coefficients for each pair of spectral bands, a, b and c are calibration

6

parameters that are obtained as described in Labergue et al [23], and R_{f120} and R_{f320} are the fluorescence ratio references measured at a known temperature T_0.

The fluorescent dye we used in this study is sulforhodamine-B dissolved in deionized water at a concentration of 5.10^{-6} mol/l. The first, second and third spectral bands are, respectively, [535-545] nm, [615-700] nm, and [555-570] nm. The uncertainty of the 3cLIF thermometry depends not only on the uncertainties of the fluorescence ratios but also on calibration parameters and the number of collected droplets. In the present work, the uncertainty analysis is similar to the performed by Labergue et al [23] and therefore, we find a statistical error of the fluorescence ratios of 1%, which leads to a droplet temperature uncertainty of $5\,^{\circ}$C.

Finally, Infrared Thermography (IRT) was used to measure the wall temperature at the outer surface of Part II, which was spray-painted to avoid the surface oxidation at high temperature and to provide a constant emissivity of 0.83. The device is a CEDIP® JADE III IR camera with spectral band of [3.7-5.1] μm equipped with a spectral filter of [3.97-4.01] μm. The following assumptions were made for the IRT analysis and the estimation of the heat dissipation by the internal two-phase flow:

- The tube temperature T_w is considered uniform in the radial direction. This assumption is supported by calculating the Biot number Bi using the tube thickness $w_t = 0.57$ mm and a heat transfer coefficient of $h_{int} = 250$ W/(m²K), which is higher than the highest value found in the Leidenfrost regime in the present study:

$$Bi = \frac{h_{int}w_t}{k_t} = \frac{250.0.57.10^{-3}}{12} = 0.012 \tag{2}$$

  where k_t is the Inconel-625 thermal conductivity at $200\,^{\circ}$C. Hence, Bi $\ll 0.1$ for all the test conditions.

- The tube temperature does not vary in the azimuthal direction, the surface temperature profile was measured along the tube centerline and we considered this profile axisymmetric.

- The tube length is 170 mm, but only the central 100 mm long were analyzed to eliminate border effects caused by the electrical contacts, which act as heat sinks. Therefore, the temperature gradient in the axial direction is very low and, consequently, thermal losses by conduction become negligible.

Before every experiment, we performed an *in-situ* calibration of the IR camera by comparing temperature measurements using a type-K thermocouple welded in the middle of the tube with IRT output signals (digital levels) taken from pixels near the thermocouple position. Then, using Planck's law, a fitting curve was obtained correlating these parameters with a maximum deviation of $5\,^{\circ}$C between IRT and thermocouple measurements, which is considered as the IRT uncertainty for the wall temperature in the present study.

The total heat flux dissipated by the internal steam-droplets flow ϕ_{int} is the sum of four contributions, as described by several models of dispersed flow film boiling in LOCA conditions [25–27]: wall-to-steam convection, wall-to-steam radiation, wall-to-droplets radiation and wall-to-droplets heat transfer by droplets impact. Each contribution can only be evaluated either by modeling or numerical simulation. Nevertheless, ϕ_{int} can still be found experimentally without determining the contribution by each path. This is possible by measuring the wall temperature during the

cooling and using an energy balance as shown in Fig. 4. In this work, using the IRT data for the wall temperature change with time, we estimated ϕ_{int} at each position z and time t with the following expression:

$$\phi_{int}(z,t) = -\left(\frac{S_t \rho_w C_{p,w}}{\pi D_{int}}\right)\frac{dT_w(z,t)}{dt} - \left(\frac{D_{ext}}{D_{int}}\right)\phi_{loss}(z,T_w) + \frac{\rho_0 I^2}{\pi D_{int} S_t} \tag{3}$$
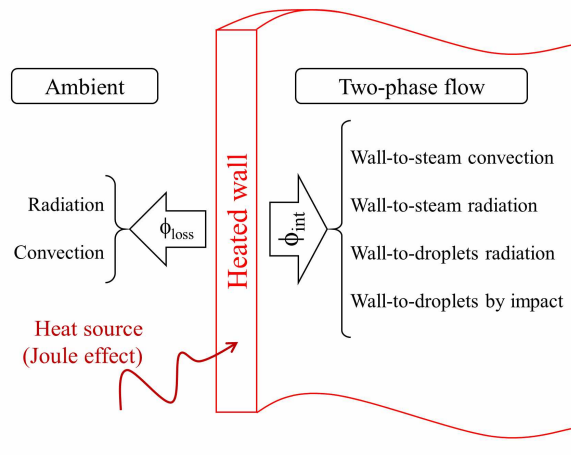

Figure 4: Energy balance to estimate the internal heat dissipation with Eq. 3.

where S_t is the tube cross-sectional area, ρ_w and $C_{p,w}$ are, respectively, the density and the specific heat of Inconel-625, D_{int} and D_{ext} are the tube internal and external diameter, and ϕ_{loss} is the heat loss to the environment by radiation and natural convection, which was validate as shown in a previous study [1]. The last term in the equation refers to the maintained heating power, which is the heat source generated by Joule effect to simulate the residual power during a LOCA, where ρ_0 is the Inconel-625 electrical resistivity and I is the electrical current during the cooling phase. For the experiments investigating only the steam flow rate effect, there is no electrical current so $I = 0$ and this source term is zero. The uncertainty of ϕ_{int} is 10%, found by error propagation of each parameter in Eq. 3.

2.4. Test procedure

Figure 5 presents the test procedure in a schematic temporal graph. First, the superheated steam flow is started to heat the pipes and the test section. Next, Part II is uniformly heated by Joule effect until reaching an almost constant initial temperature above $600\,°C$ and then we start the droplets injection. At this point, we measure the droplets diameter and velocity upstream of Part II with the PDA system and the droplets temperature up- and downstream of Part II with 3cLIF thermometry. Finally, the current supplied by the DC generator is reduced to a constant value that results in the desired maintained heating power in the heated tube (from 0 to 2 kW/m) that is, in its turn, estimated by Joule effect using Inconel-625 electrical resistivity. At this moment, the cooling-phase experiment begins, recording simultaneously the wall temperature with IRT and the droplets diameter and velocity downstream of Part II with PDA. After enough time for the wall to cool down and have its temperature stabilized (limited to 120 s), the experiment is finished. For information, Table 1 presents the ranges of the experimental conditions in this study.
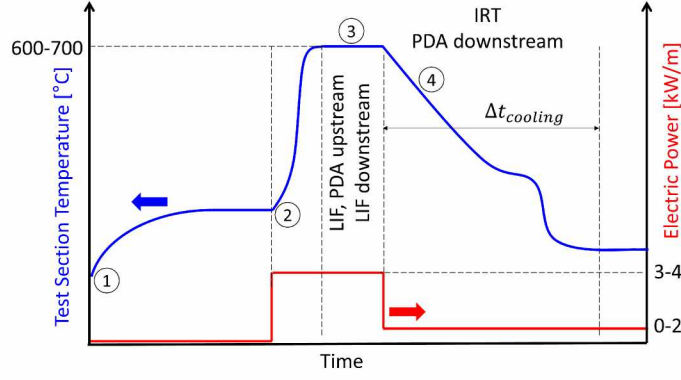
8

Figure 5: Test procedure and its steps: (1) starting of the steam flow; (2) heating of the test section and starting of the droplets injection; (3) droplets characteristics measured by PDA and LIF; (4) cooling-phase experiment with IRT and PDA.

Table 1: Range of the experimental conditions.

Parameter	Range
Steam pressure	$1.0 - 1.4$ bar
Mass flow rate of injected droplets	0.8 kg/h
Droplets temperature at injection	$61 - 62.5\,°C$
Droplets diameter upstream of Part II	$5 - 300\ \mu m$
Steam mass flow rate	$2.1 - 7.5$ kg/h
Steam temperature upstream of Part II	$144 - 195\,°C$
Volumetric fraction of droplets	$5.10^{-5} - 2.10^{-4}$
Initial mean wall temperature	$597 - 650\,°C$
Maintained heating power	$0 - 2$ kW/m

3. Results and discussion: effect of the steam flow rate

Before presenting and discussing the test results, we must define two types of mean values used in this study. The first one, which is applied only for the wall temperature T_w, is the spatial mean value $\overline{T}_w$ of the wall temperature profile $T_w(z)$ expressed by:

$$\overline{T}_w = \frac{\sum_{k=1}^{N_w} T_{w,k}(z)}{N_w} \tag{4}$$

where N_w is the number of pixels from the IRT along the tube axis at a time t during the cooling phase. The second one is the classic arithmetic mean $\widetilde{x}$ of an arbitrary parameter x, which is defined by:

$$\widetilde{x} = \frac{\sum_{k=1}^{N} x_k}{N} \tag{5}$$

with N being the amount of data of the population in analysis.

In this section, we present the results for different steam flow rates, starting with the analysis of the flow entering the heated tube and then presenting the results using each measurement technique. Results regarding the effect of the maintained heating power are found in section 4.

9

3.1. Flow and wall condition before the cooling phase

Table 2 shows the flow conditions upstream of Part II and the initial wall temperature for each experiment, while Fig. 6 presents PDA results of the droplets characteristics also upstream of Part II. The steam velocity $\widetilde{u}_s$ is estimated by mass balance:

$$\widetilde{u}_s = \frac{4\dot{m}_s}{\rho_s \pi D_h^2} \tag{6}$$

where $\dot{m}_s$ is the steam mass flow rate measured by a flowmeter and ρ_s is the steam density at a temperature $\widetilde{T}_s$, which is, in its turn, the steam temperature upstream of Part II measured by a thermocouple.

Table 2: Flow conditions upstream of Part II and initial wall temperature before the cooling experiment.

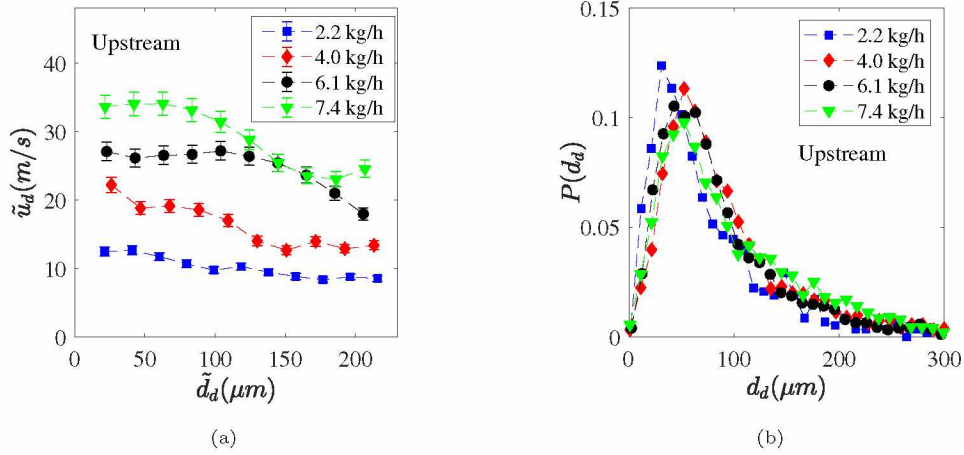| $\widetilde{\dot{m}}_s$	$\widetilde{T}_s$	$\widetilde{u}_d$	$\widetilde{d}_d$	$\widetilde{u}_s$	$\overline{T}_w(t=0)$
2.2 kg/h	150 °C	11.5 m/s	83 μm	10.9 m/s	638 °C
4.0 kg/h	165 °C	14.5 m/s	105 μm	20.5 m/s	627 °C
6.1 kg/h	190 °C	23.0 m/s	98 μm	33.0 m/s	635 °C
7.4 kg/h	195 °C	29.5 m/s	101 μm	40.5 m/s	650 °C

Figure 6: Droplets characteristics upstream of Part II for each steam flow rate: (a) droplets velocity as a function of their diameter; (b) droplets diameter distribution.

The droplets velocity is higher with the increase in the steam flow rate, which was expected because the steam velocity is also higher (as shown in Table 2) and, as a result, the droplets are accelerated by the steam. This result represents correctly LOCA conditions as well as other applications where droplets are entrained by the steam. For all the steam flow rates, smaller droplets have higher velocity than the larger ones, as shown in Fig. 6a. A nearly uniform profile is observed for 2.2 kg/h steam flow rate, although there is a slight trend of larger droplets being slower. In contrast, the mean droplets diameter is approximately the same regardless of the steam flow rate (Table 2), as well as their distribution (Fig. 6b). This is important to mention that the droplets characteristics upstream of Part II (both diameter and velocity) are nearly constant throughout the cooling process.

Finally, the steam temperature at the inlet is higher for higher steam flow rates (Table 2). This is because of heat losses to the ambient, even though thermal insulation is used on the pipes. Indeed, steam exiting the superheater at a lower velocity has a longer transit time in the pipeline and, consequently, undergoes a larger temperature decrease and enters in the test section at a lower temperature. Although there is this temperature difference at the inlet of the test section, the comparison of the test results to evaluate the steam flow rate effect is still valid since the variation in the steam flow rate is much more significant than the change in its temperature or than the change in the difference between the wall and steam temperatures. This is confirmed by the results presented in the next sections.

3.2. IRT results: internal heat dissipation and wall rewetting

Figure 7 presents the spatiotemporal variation in the tube temperature T_w and the heat flux ϕ_{int} dissipated by the steam-droplets flow. For all the cases, there is an instant when the wall temperature sharply decreases, followed by an increase in the local heat dissipation. This happens because of wall rewetting, which occurs when the droplets impinge onto the wall and wet it instead of bouncing away. Even though the flow is in a straight tube, droplets experience transversal velocities because of the turbulent flow – for instance, the lowest steam Reynolds number among the test cases, i.e. for 2.2 kg/h steam flow rate, is approximately 4450. During the Leidenfrost regime, droplets impact contributes significantly to the heat dissipation, as already discussed by several authors [25–27], until the vapor layer eventually breaks and the liquid wets the surface, increasing substantially the heat dissipation.

The rewetting front position, represented by dashed black lines on the maps, is estimated by calculating the second derivative of the wall temperature with time at each location and finding each minimum value [28]. In general, rewetting occurs from bottom to top. Specifically for the steam flow rate of 2.2 kg/h, rewetting began almost instantaneously at the bottom and in the middle of the tube, rapidly spreading to all over the length. This specific result is discussed further in this section. Furthermore, rewetting occurs earlier with higher steam flow rates. This was expected because wall rewetting occurs at lower wall temperatures, which is reached faster with higher steam flow rates due to enhanced heat dissipation by forced convection.

Figure 8 presents mean boiling curves for each steam flow rate. To obtain this plot, temperature points in the maps shown in Figure 7 were taken within ranges of $10\,°C$ and their corresponding internal heat flux. Then, we calculated the arithmetic mean for each group of temperature and heat flux using Eq. 5, resulting in the points presented in Fig. 8. Notice that these mean values of heat flux $\widetilde{\phi}_{int}$ and wall temperature $\widetilde{T}_w$ are not mean axial values at each instant, but mean values of the amount of data from the spatiotemporal maps within each temperature range. This value of $10\,°C$ for the range was chosen for a better analysis and comparison of the test results and it does not affect significantly the uncertainties of wall temperature and heat flux because the statistical errors of the mean value calculation are negligible. Hence, the uncertainties of the temperature and heat flux in Fig. 8 are still $5\,°C$ and 10%, respectively.

For all the cases, the heat flux decreases as the wall temperature decreases during the Leindenfrost regime until a minimal point where wall rewetting takes place (inflection point). It is important to remind that this minimal heat flux is not equivalent to the Leidenfrost heat flux, because, as shown in Fig. 4, ϕ_{int} is a summation of several heat transfer contributions. Moreover, wall rewetting occurs at a higher temperature for higher steam flow rates because droplets flow at higher velocities (which is confirmed with PDA results in section 3.3) and, therefore, have higher
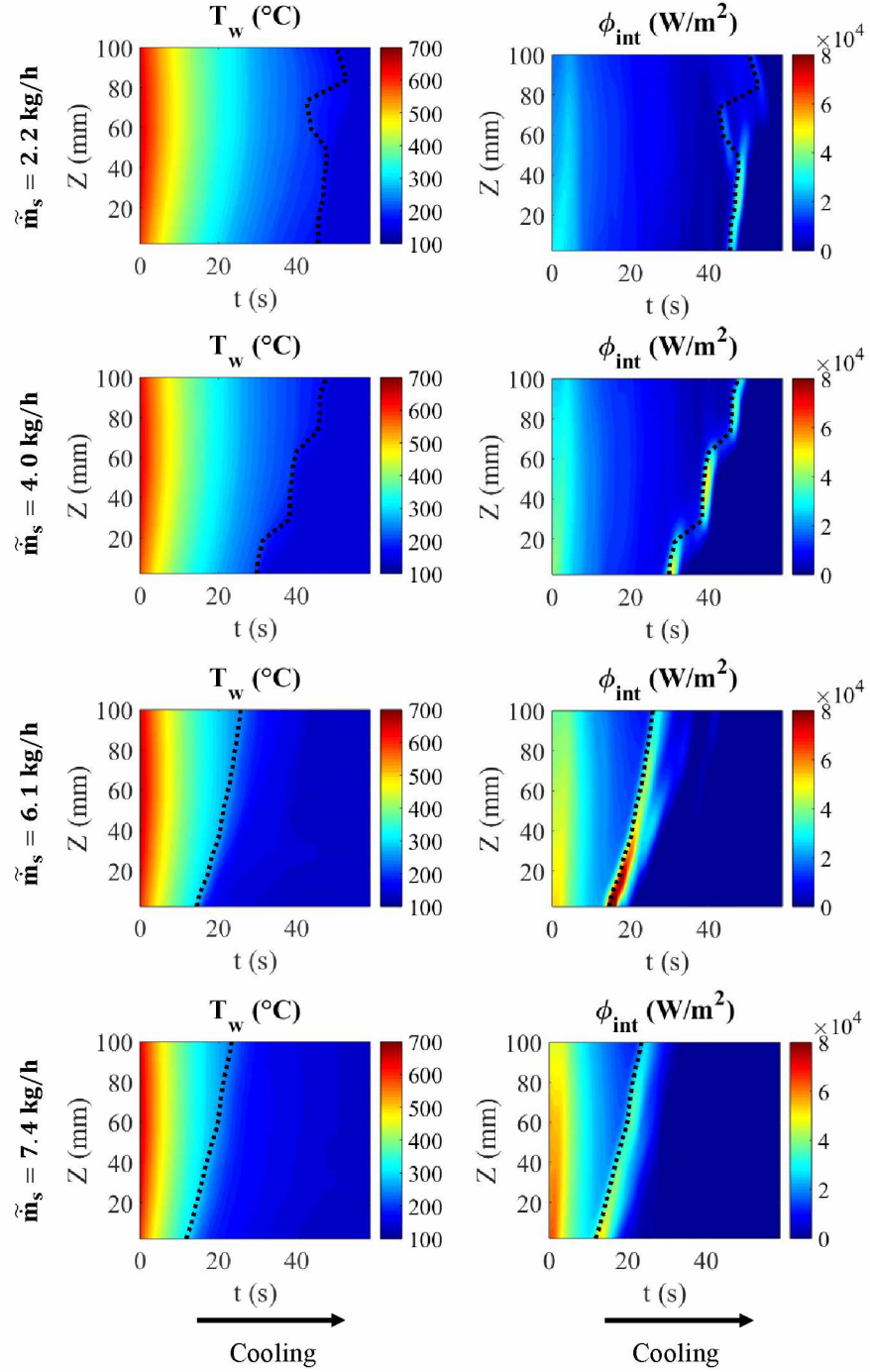
11

Figure 7: Spatiotemporal maps of temperature and heat flux dissipated by the internal two-phase flow for each steam flow rate, and the evolution of the rewetting front (dotted line).

kinetic energy. Dunand et al [29] observed a similar behavior by impinging droplets onto a heated wall, confirming that droplets with higher Weber number of impact tend to rewet the surface at higher temperatures.

Resuming the discussion on the wall rewetting behavior with 2.2 kg/h in Fig. 7, this might have happened because, at this flow rate, droplets velocity is very low (as shown in the next section) and, consequently, their kinetic energy when impacting onto the surface is also very low. For this reason, wall rewetting only occurs at lower temperatures,
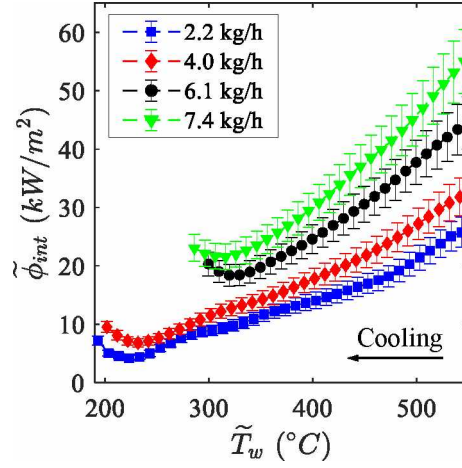
Figure 8: Heat flux as a function of the wall temperature for each steam flow rate.

as observed in Fig. 8. In fact, the wall rewetting temperature for 2.2 kg/h is approximately $220\,^{\circ}\mathrm{C}$, which is close usual values of the Leidenfrost temperature found in the literature with sessile droplets onto smooth metallic hot surfaces [30–32]. Then, once one droplet wets the wall, the temperature close to this location decreases to values below the Leidenfrost temperature and the rewetting front quickly spreads over the surface.

In section 2.3, we mentioned the hypotheses of constant temperature of the tube in the azimuthal direction and negligible conductive heat transfer to estimate the internal heat dissipation by Eq. 3. Nevertheless, as discussed in our previous study [1], the rewetting front does not always progress uniformly, as Fig. 9 for a steam flow rate of 6.1 kg/h. Downstream of the rewetting front, the tube temperature is nearly homogeneous in the azimuthal direction and the gradient in the axial direction is very low, which means that the heat flux estimated by Eq. 3 is accurate during the Leidenfrost regime. However, at the rewetting front, we observe high temperature gradients in both the azimuthal and axial directions. Consequently, as conductive heat transfer is not considered in the calculation, Eq. 3 overestimates the heat dissipation near the minimum heat flux point in Fig. 8.
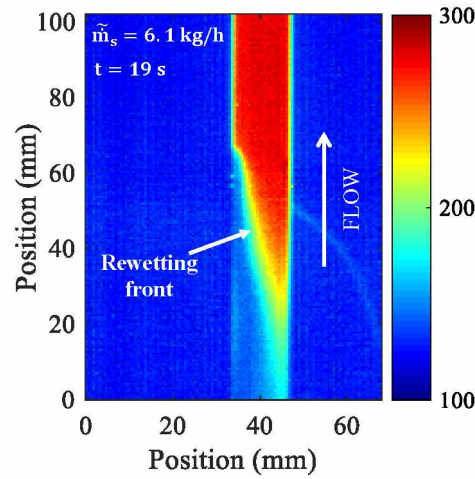

Figure 9: IRT image of the wall temperature for 6.1 kg/h steam flow rate at t = 19 s showing a non-uniform progress of the rewetting front in the tube.

3.3. PDA results: droplets characteristics

Figure 10a shows the droplets diameter distribution downstream of Part II, where no significant difference is observed for the different test cases. In fact, the mean droplets diameter is 65 μm, 85 μm, 68 μm, and 70 μm for steam flow rates of 2.2 kg/h, 4.0 kg/h, 6.1 kg/, and 7.4 kg/h, respectively. Comparing these values with the condition upstream of the heated tube (Table 2), we find a reduction in the droplets diameter by 23% to 30%, which occurs due to heat transfer from both wall and steam to droplets that results in their evaporation, as discussed by Oliveira et al [25]. Droplets breakup does not occur in any case because their Weber number never reaches the critical value of 12 [33], as shown in Fig. 11. The droplets Weber number is calculated by:

$$We_d = \frac{\rho_s \left(\widetilde{u}_s - u_d\right)^2 d_d}{\sigma_d} \tag{7}$$

where u_d and d_d are the droplet velocity and diameter obtained by PDA measurements upstream of the tube (Figure 6a), and σ_d is the liquid surface tension. Meanwhile, Figure 10b presents the variation in the droplets velocity with their diameter for each steam flow rate when the mean axial wall temperature is within the range $400\,^\circ\mathrm{C} < \overline{T}_w < 500\,^\circ\mathrm{C}$. We remind that it is possible to specify the droplets characteristics within a range of wall temperature because IRT and PDA results are synchronized. Comparing the droplets velocities up- and downstream of Part II, there is a considerable increase along the heated tube because of the steam acceleration due to heating. This is easily observed for smaller droplets, whose inertia is very low and they are easily entrained by the steam flow. For this reason, smaller droplets have higher velocity compared to larger droplets.
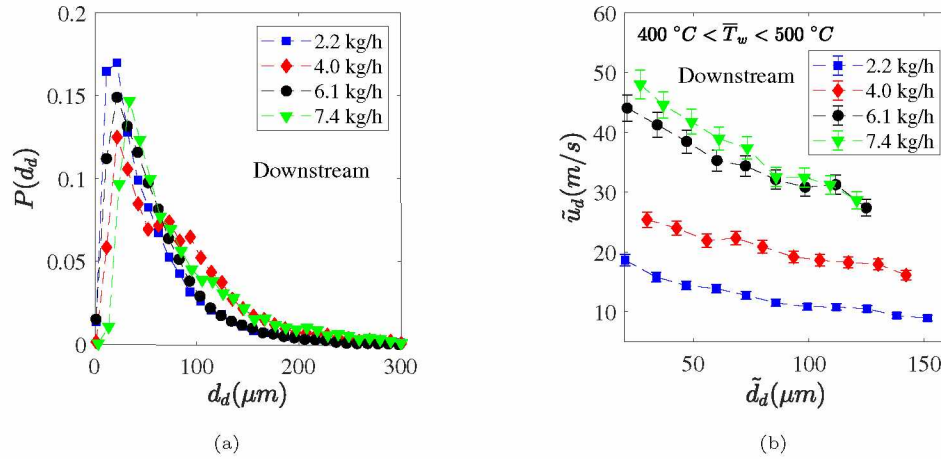

Figure 10: a) Droplet diameter distribution and b) velocity downstream of Part II for each steam flow rate and for the wall temperature range of $400\,^\circ\mathrm{C} < \overline{T}_w < 500\,^\circ\mathrm{C}$.

Again because of the synchronized PDA and IRT measurements, we can also correlate the droplets characteristics with the wall temperature as presented in Fig. 12a for the mean droplets diameter and in Fig. 12b for the mean droplets velocity. On the one hand, the droplets diameter does not vary significantly with the wall temperature for the two highest steam flow rates, while it tenuously decrease through the cooling phase for the lowest steam flow rates (i.e. 2.2 kg/h and 4.0 kg/h). On the other hand, the droplets velocity decreases with the decrease in the wall temperature for the highest steam flow rates (i.e. 6.1 kg/h and 7.4 kg/h). This trend occurs because the steam
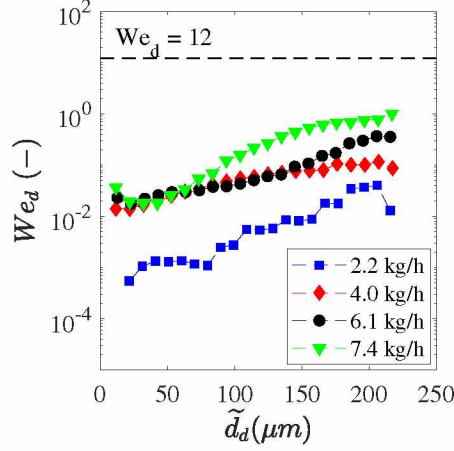
Figure 11: Droplets Weber number as a function of their diameter.

heating is less intense for lower wall temperatures and, consequently, it is less accelerated in Part II. For 2.2 kg/h and 4.0 kg/h steam flow rates, the droplets velocity is nearly constant throughout the cooling phase because the difference between the steam and the droplets velocities is not large and, by consequence, the mean droplets velocity does not change substantially.
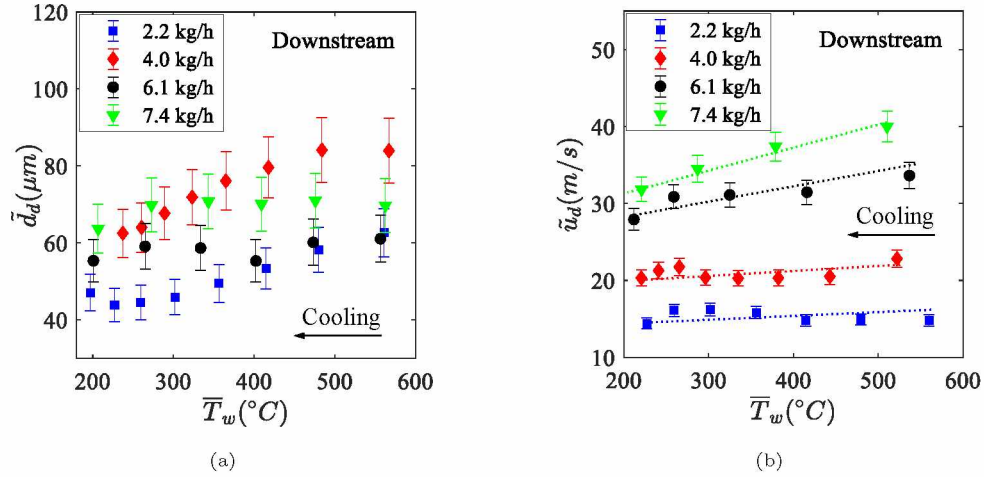

Figure 12: Variation in the droplets characteristics with the wall mean axial temperature for each steam flow rate. (a) droplets diameter; (b) droplets velocity.

3.4. 3cLIF results: droplets temperature

Because the amount of droplets collected by the 3cLIF thermometry is much less compared with the PDA system (a few hundred against several thousand, respectively), we were not able to measure the transient of the droplets temperature. Hence, this measurement was performed up- and downstream Part II before starting the cooling phase (moment 3 in Fig. 5). Table 3 presents these results for each steam flow rate.

Despite the droplets are injected at 62 °C (Table 1), they reach Part II at a temperature approximately 20 °C higher because they are heated by the steam flow. This probably occurs in the steam-droplets mixer upstream of Part I, where there is intense turbulence and, consequently, intense heat exchange between the dispersed and continuous

15

Table 3: Mean droplet temperature upstream and downstream part II using LIF technique.

$\widetilde{m}_s$	$\widetilde{T}_d$ (upstream)	$\widetilde{T}_d$ (downstream)
2.2 kg/h	81 °C	84 °C
4.0 kg/h	79 °C	82 °C
6.1 kg/h	80 °C	85 °C
7.4 kg/h	82 °C	85 °C

phases. Nevertheless, droplets mean volume temperature does not change considerably after passing through Part II, regardless of the steam flow rate. Although there is an average increase by 3 °C (Table 3), this difference is still within the 3cLIF uncertainty of 5 °C and, hence, is not statistically significant.

Notice that droplet evaporation still takes place, as observed in the results of droplets diameter reduction discussed in section 3.3, even though the droplets temperature is below saturation. This happens because the droplet's surface heats faster than it is diffused to its volume, as observed by Strizhak et al [34] and Sazhin et al [35]. Consequently, mass evaporates without substantial increase in the droplets mean volume temperature, which is consistent with the present results.

4. Results and discussion: effect of the maintained heating power

In this second part of the experimental results, all the test parameters are fixed except the maintained heating power during the cooling phase to evaluate its effect. Here, the flow conditions are: steam flow rate of 4.1 kg/h, steam temperature upstream of Part II of 165 °C, and droplets flow rate of 0.8 kg/h. Four different maintained heating powers during the cooling phase were tested, from 0.5 kW/m to 2.0 kW/m, and also with no heating, as shown in Fig. 5 and presented as the last term in Eq. 3. Table 4 presents the mean droplets diameter and velocity upstream of Part II for each scenario, showing that the inlet conditions are very similar. Therefore, we can evaluate separately the maintained heating power effect on the thermal-hydraulics of the dispersed flow film boiling.

Table 4: Mean droplets diameter and velocity upstream of Part II for each maintained heating power (M.H.P.).

M.H.P. [kW/m]	0	0.5	1.0	1.5	2.0
$\widetilde{d}_d$ [μm]	89	90	92	86	94
$\widetilde{u}_d$ [m/s]	15.6	15.0	15.4	15.5	16.0

Starting with the IRT results, Fig. 13 presents the spatiotemporal maps (temperature and internal heat flux) for each maintained heating power. For all the cases, the temperature decreases in the course of the cooling phase; however, as expected, the wall cooling is slower with the increase in the maintained heating power. The most important observation from these results is that wall rewetting does not occur for maintained heating powers higher than 1.5 kW/m throughout the duration of the experiments (about 120 s). This happens because the heat generated in these cases is high enough to keep the wall temperature much above the Leidenfrost temperature and, consequently,

droplets impinge onto the wall and rebound. Contrarily, droplets eventually rewet the wall for lower and no maintained heating power conditions. Similarly to the observed when analyzing the steam flow rate effect, rewetting front progresses from bottom to top; however, it takes longer to cover the whole internal surface of the tube for higher maintained heating powers.
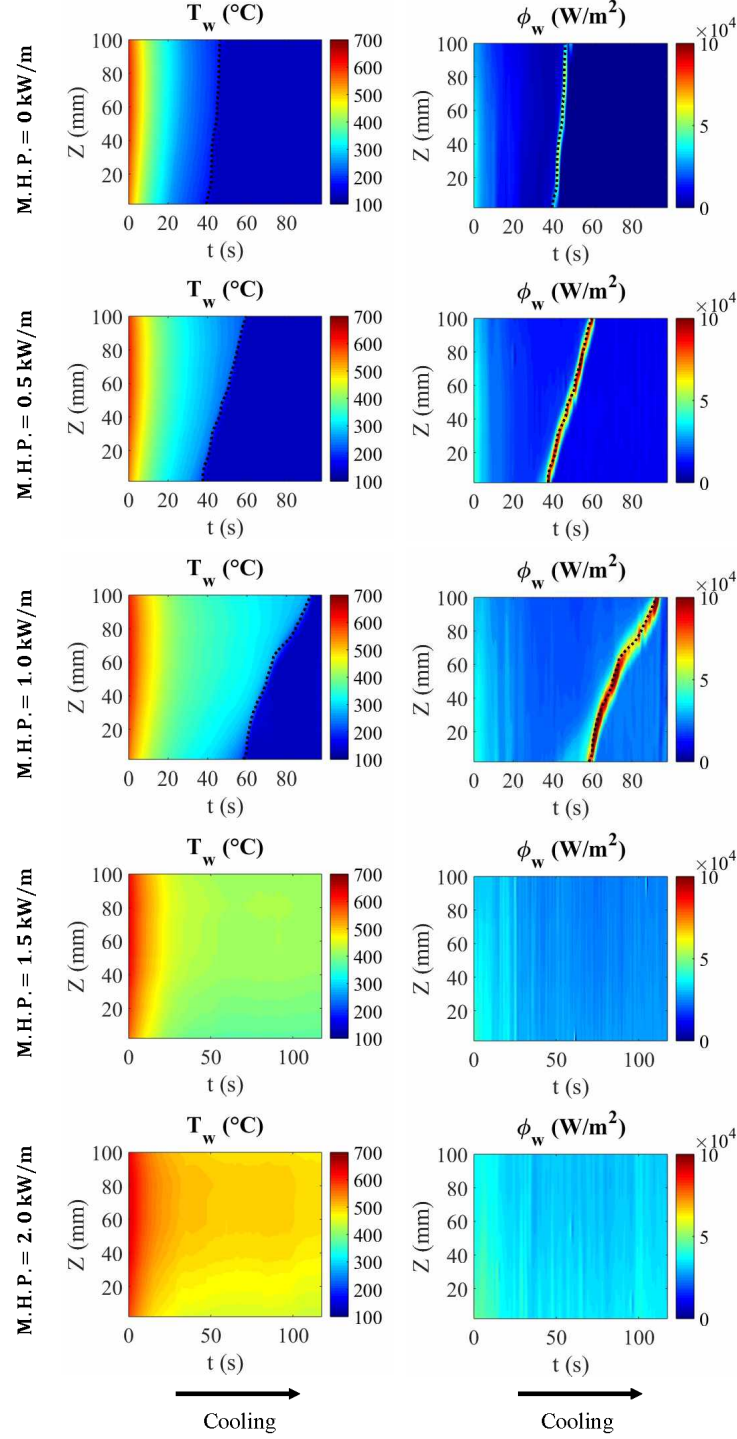

Figure 13: Spatiotemporal maps of temperature and heat flux dissipated by the internal two-phase flow for each maintained heating power (M.H.P.), and the evolution of the rewetting front (dotted line) where applicable.

Meanwhile, Fig. 14 presents the boiling curves for all the cases, which were obtained using the same method explained before for Fig. 8 and, hence, the same discussion of high temperature gradients at the rewetting front location and overestimation of the internal heat dissipation near the minimum heat flux is still valid. The internal heat dissipation is nearly the same during the Leidenfrost regime (before wall rewetting), regardless of the maintained heating power, which was expected as the flow condition is always the same. From this graph, we can notice again that wall rewetting only occurs for the cases without heating and with maintained heating powers of 0.5 and 1.0 kW/m. One interesting point is that wall rewetting takes place at higher temperatures with the increase in the maintained heating power. The reason for this result is still unclear and deserves further investigation.
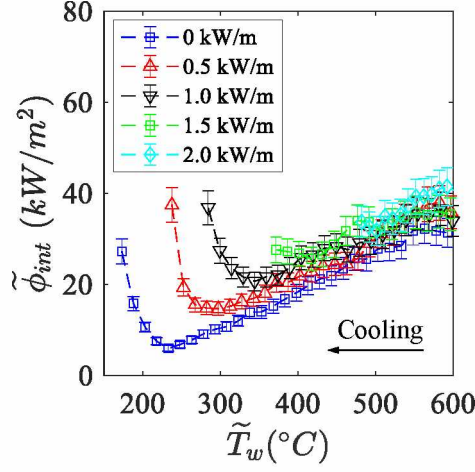

Figure 14: Heat flux as a function of the wall temperature for each maintained heating power.

Regarding the droplets characteristics downstream of Part II, Figs. 15a and 15b show respectively their mean diameter and velocity as a function of the wall mean temperature. Likewise observed upstream of the heated tube, the droplets dynamics are basically the same for all the maintained heating powers. Also, similarly to the results varying the steam flow rate, both the droplets diameter and velocity decrease during the cooling phase.
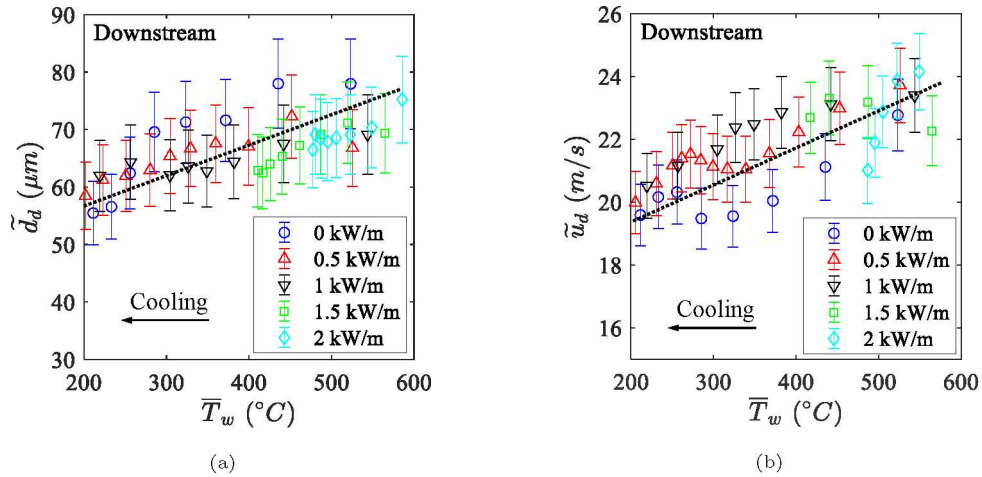

(a)

(b)

Figure 15: Variation in the droplets characteristics with the wall mean axial temperature for each maintained heating power. (a) droplets diameter; (b) droplets velocity.

The mean droplets temperature was not measured in these experiments because, as already explained, we could

not perform a transient measurement, impeding an analysis of the maintained heating power effect on this parameter.

5. Conclusions

A dedicated experimental rig was built for thermal-hydraulic studies in dispersed flow film boiling at a sub-channel scale in LOCA conditions. In this study, the effects of the steam flow rate and the maintained heating power on the cooling process of a vertical heated tube were analyzed. Using synchronized optical techniques to measure the wall temperature and the droplets characteristics, the heat dissipation by the internal flow was estimated and the droplets velocity and diameter evolution was correlated to the wall temperature. These experimental results provide valuable data for the validation of mechanistic models and simulation tools.

Results showed that wall rewetting generally starts from bottom to top, although it took place almost instantaneously along the tube for 2.2 kg/h steam flow rate, which is the lowest value in this study. A possible reason is droplets velocity is very low when impinging onto the heated wall, so it wets the wall at lower temperatures. Hence, when one droplet wet the surface, the wall temperature near this position decreases below the Leidenfrost temperature and the rewetting front spreads faster. Moreover, wall rewetting occurs earlier for higher steam flow rates. If the maintained heating power during the cooling phase is high enough (higher than 1.5 kW/m with the selected steam-droplets flows in the present work), droplets cannot rewet the wall for a relatively long period (120 s in these experiments). Otherwise, wall rewetting takes place but progresses slower compared to the case with no heating power. Because of the higher droplets kinetic energy, wall rewetting occurs at higher wall temperatures with the increase in the steam flow rate. Also, wall rewetting temperature increases with the increase in the maintained heating power, a result that needs further investigation.

Regarding the droplets characteristics, their diameter reduces by 23% to 30% downstream of the heated tube compared to upstream values. This happens because of the heat transfer from wall and steam to droplets, resulting in their evaporation. Furthermore, the droplets diameter does not vary significantly through the cooling phase for higher steam flow rate, while there is a slight decreasing trend for lower steam flow rates. Contrarily, for higher steam flow rates, the droplets velocity is highly influenced by the wall temperature and it decreases in the course of the cooling phase. Also, the droplets velocity increases after passing the heated tube due to acceleration of the steam flow. Finally, the droplets mean volume temperature does not change significantly from up- to downstream of the heated tube, even though droplets evaporation takes place at the liquid surface.

6. Acknowledgments

References

[1] J. D. Peña Carrillo, A. V. S. Oliveira, A. Labergue, T. Glantz, M. Gradeck, Experimental thermal hydraulics study of the blockage ratio effect during the cooling of a vertical tube with an internal steam-droplets flow,

International Journal of Heat and Mass Transfer 140 (2019) 648 – 659. `doi:https://doi.org/10.1016/j.ijheatmasstransfer.2019.06.012`.

[2] C. Grandjean, Coolability of blocked regions in a rod bundle after ballooning under loca conditions: Main findings from a review of past experimental programmes, Nuclear Engineering and Design 237 (15) (2007) 1872 – 1886, NURETH-11. `doi:https://doi.org/10.1016/j.nucengdes.2007.02.022`.

[3] G. Repetto, C. Dominguez, B. Durville, S. Carnemolla, D. Campello, C. Tardif, M. Gradeck, The R&D PER-FROI project on thermal mechanical and thermal hydraulics behaviors of a fuel rod assembly during a loss of coolant accident, International Topical Meeting on Nuclear Reactor Thermal Hydraulics 2015, NURETH 2015 1 (2015) 1–14.

[4] K. Kim, B. J. Kim, H. S. Choi, S. K. Moon, C. H. Song, Effect of a blockage length on the coolability during reflood in a 2 x 2 rod bundle with a 90% partially blocked region, Nuclear Engineering and Design 312 (2017) 248–255. `doi:10.1016/j.nucengdes.2016.08.031`.

[5] P. Ruyer, N. Seiler, B. Biton, F. Lelong, F. Secondi, D. Baalbaki, M. Gradeck, Two-phase flow across a partially damaged core during the reflood phase of a LOCA, Nuclear Engineering and Design 264 (2013) 187 – 194, sI:NURETH-14. `doi:https://doi.org/10.1016/j.nucengdes.2013.02.026`.

[6] R. Lee, J. Reyes, K. Almenas, Size and number density change of droplet populations above a quench front during reflood, International Journal of Heat and Mass Transfer 27 (4) (1984) 573 – 585. `doi:https://doi.org/10.1016/0017-9310(84)90030-9`.

[7] R. Sindhuja, A. Balakrishnan, S. S. Murthy, Post-CHF heat transfer during two-phase upflow boiling of R-407C in a vertical pipe, Applied Thermal Engineering 30 (2) (2010) 167 – 173. `doi:https://doi.org/10.1016/j.applthermaleng.2009.07.016`.

[8] T. Karayiannis, M. Mahmoud, Flow boiling in microchannels: Fundamentals and applications, Applied Thermal Engineering 115 (2017) 1372 – 1397. `doi:https://doi.org/10.1016/j.applthermaleng.2016.08.063`.

[9] Z.-H. Li, Y. Wang, D.-N. Jia, P.-X. Jiang, Dispersed flow film boiling in vertical narrow annular gaps, Applied Thermal Engineering 29 (5) (2009) 1146 – 1152. `doi:https://doi.org/10.1016/j.applthermaleng.2008.06.008`.

[10] M. M. Shah, Comprehensive correlation for dispersed flow film boiling heat transfer in mini/macro tubes, International Journal of Refrigeration 78 (2017) 32 – 46. `doi:https://doi.org/10.1016/j.ijrefrig.2017.03.019`.

[11] G. Liang, I. Mudawar, Review of spray cooling – part 2: High temperature boiling regimes and quenching applications, International Journal of Heat and Mass Transfer 115 (2017) 1206 – 1222. `doi:https://doi.org/10.1016/j.ijheatmasstransfer.2017.06.022`.

[12] Y. Wang, Y. Jiang, W. Chen, B. Zhou, Heat transfer characteristics of spray cooling beyond critical heat flux under severe heat dissipation condition, Applied Thermal Engineering 123 (2017) 1356 – 1364. `doi:https://doi.org/10.1016/j.applthermaleng.2017.04.165`.

[13] M. Gradeck, N. Seiler, P. Ruyer, D. Maillet, Heat transfer for leidenfrost drops bouncing onto a hot surface, Experimental Thermal and Fluid Science 47 (2013) 14 – 25. `doi:https://doi.org/10.1016/j.expthermflusci.2012.10.023`.

[14] Y. Jin, F.-B. Cheung, S. M. Bajorek, K. Tien, C. L. Hoxie, Investigation of the thermal-hydraulic non-equilibrium in a 7x7 rod bundle during reflood, International Journal of Heat and Mass Transfer 127 (2018) 266 – 279. `doi:https://doi.org/10.1016/j.ijheatmasstransfer.2018.08.011`.

[15] J. Kim, S. Cho, J.-K. Park, Y.-J. Youn, S.-K. Moon, Experimental study to assess effects of ballooning and fuel relocation on the coolability of fuel rod bundle, Nuclear Engineering and Design 332 (2018) 1 – 10. `doi:https://doi.org/10.1016/j.nucengdes.2018.03.013`.

[16] Y. Liu, D. Cui, J. Lin, J. Liu, C. Li, S. Huang, Z. Xiong, H. Yin, Experimental study on steady-state heat transfer characteristics of the nozzle-atomized dispersed flow, Applied Thermal Engineering 140 (2018) 686 – 695. `doi:https://doi.org/10.1016/j.applthermaleng.2018.05.067`.

[17] T. Glantz, T. Taurines, S. Belon, O. D. Luze, G. Guillard, F. Jacq, Draccar: A multi-physics code for computational analysis of multi-rod ballooning, coolability and fuel relocation during loca transients. part two: Overview of modeling capabilities for loca, Nuclear Engineering and Design 339 (2018) 202 – 214. `doi:https://doi.org/10.1016/j.nucengdes.2018.08.031`.

[18] T. Glantz, T. Taurines, O. D. Luze, S. Belon, G. Guillard, F. Jacq, Draccar: A multi-physics code for computational analysis of multi-rod ballooning, coolability and fuel relocation during loca transients. part one: General modeling description, Nuclear Engineering and Design 339 (2018) 269 – 285. `doi:https://doi.org/10.1016/j.nucengdes.2018.06.022`.

[19] J. D. Peña Carrillo, M. Gradeck, A. Labergue, T. Glantz, Identification of heat transfers for a vapor-droplets flow inside a representative fuel assembly subchannel - experimental and model approach, in: Proceedings of the 16th International Heat Transfer Conference, IHTC-16, 2018, pp. 6665–6672. `doi:10.1615/IHTC16.mpf.022179`.

[20] H. Albrecht, N. Damaschke, M. Borys, C. Tropea, Laser Doppler and Phase Doppler Measurement Techniques, Experimental Fluid Mechanics, Springer-Verlag Berlin Heidelberg, 2003.
URL `https://www.springer.com/la/book/9783540678380`

[21] A. Labergue, J.-D. Pena-Carillo, M. Gradeck, F. Lemoine, Combined three-color LIF-PDA measurements and infrared thermography applied to the study of the spray impingement on a heated surface above the leidenfrost regime, International Journal of Heat and Mass Transfer 104 (2017) 1008 – 1021. `doi:https://doi.org/10.1016/j.ijheatmasstransfer.2016.07.029`.

[22] A. Labergue, A. Delconte, F. Lemoine, Study of the thermal mixing between two non-isothermal sprays using combined three-color lif thermometry and phase doppler analyzer, Experiments in Fluids 54 (6) (2013) 1527. doi:https://doi.org/10.1007/s00348-013-1527-1.

[23] A. Labergue, A. Delconte, G. Castanet, F. Lemoine, Study of the droplet size effect coupled with the laser light scattering in sprays for two-color lif thermometry measurements, Experiments in Fluids 52 (5) (2012) 1121–1132. doi:https://doi.org/10.1007/s00348-011-1242-8.

[24] A. Labergue, V. Deprédurand, A. Delconte, G. Castanet, F. Lemoine, New insight into two-color lif thermometry applied to temperature measurements of droplets, Experiments in Fluids 49 (2) (2010) 547–556. doi:https://doi.org/10.1007/s00348-010-0828-x.

[25] A. V. S. Oliveira, J. D. Peña Carrillo, A. Labergue, T. Glantz, M. Gradeck, Mechanistic modeling of the thermal-hydraulics in polydispersed flow film boiling in LOCA conditions, Nuclear Engineering and Design 357 (2020) 110388. doi:https://doi.org/10.1016/j.nucengdes.2019.110388.

[26] M. J. Meholic, D. L. Aumiller, F. B. Cheung, A comprehensive, mechanistic heat transfer modeling package for dispersed flow film boiling - Part 1 - Development, Nuclear Engineering and Design 291 (2015) 295–301. doi:10.1016/j.nucengdes.2015.07.013.

[27] Y. Guo, K. Mishima, A non-equilibrium mechanistic heat transfer model for post-dryout dispersed flow regime, Experimental Thermal and Fluid Science 26 (6-7) (2002) 861–869. doi:10.1016/S0894-1777(02)00195-4.

[28] Y. Barnea, E. Elias, I. Shai, Flow and heat transfer regimes during quenching of hot surfaces, International Journal of Heat and Mass Transfer 37 (10) (1994) 1441 – 1453. doi:https://doi.org/10.1016/0017-9310(94)90146-5.

[29] P. Dunand, G. Castanet, M. Gradeck, D. Maillet, F. Lemoine, Energy balance of droplets impinging onto a wall heated above the Leidenfrost temperature, International Journal of Heat and Fluid Flow 44 (2013) 170 – 180. doi:https://doi.org/10.1016/j.ijheatfluidflow.2013.05.021.

[30] C. Cai, I. Mudawar, H. Liu, C. Si, Theoretical leidenfrost point (lfp) model for sessile droplet, International Journal of Heat and Mass Transfer 146 (2020) 118802. doi:https://doi.org/10.1016/j.ijheatmasstransfer.2019.118802.

[31] A. V. Oliveira, D. L. Medeiros Filho, R. Gonçalves dos Santos, Determination of boiling critical temperatures of pure and binary mixtures of water and ethanol by droplet evaporation, in: Proceedings of the IV Journeys in Multiphase Flows (JEM2015), 2015.

[32] J. D. Bernardin, I. Mudawar, The Leidenfrost Point: Experimental Study and Assessment of Existing Models, Journal of Heat Transfer 121 (4) (1999) 894–903. doi:https://doi.org/10.1115/1.2826080.

[33] M. Pilch, C. Erdman, Use of breakup time data and velocity history data to predict the maximum size of stable fragments for acceleration-induced breakup of a liquid drop, International Journal of Multiphase Flow 13 (6) (1987) 741 – 757. doi:https://doi.org/10.1016/0301-9322(87)90063-2.

[34] P. Strizhak, R. Volkov, G. Castanet, F. Lemoine, O. Rybdylova, S. Sazhin, Heating and evaporation of suspended water droplets: Experimental studies and modelling, International Journal of Heat and Mass Transfer 127 (2018) 92 – 106. `doi:https://doi.org/10.1016/j.ijheatmasstransfer.2018.06.103`.

[35] S. Sazhin, P. Krutitskii, I. Gusev, M. Heikal, Transient heating of an evaporating droplet with presumed time evolution of its radius, International Journal of Heat and Mass Transfer 54 (5) (2011) 1278 – 1288. `doi:https://doi.org/10.1016/j.ijheatmasstransfer.2010.10.018`.